Magnetic skyrmion manipulation in $CrTe_2/WTe_2$ 2D van der Waals heterostructure

Sotirios Fragkos[1,2,a)], Panagiotis Pappas[1], Evgenia Symeonidou[1,3], Yerassimos Panayiotatos[2], Athanasios Dimoulas[1,a)]

[1]Institute of Nanoscience and Nanotechnology, National Center for Scientific Research "Demokritos", 15310 Athens, Greece

[2]Department of Mechanical Engineering, University of West Attica, 12241 Athens, Greece

[3]School of Chemistry, Aristotle University of Thessaloniki, 54124 Thessaloniki, Greece

[a)]Authors to whom correspondence should be addressed: s.fragkos@inn.demokritos.gr; s.fragkos@uniwa.gr; and a.dimoulas@inn.demokritos.gr

Magnetic skyrmions in two-dimensional van der Waals materials provide an ideal platform to push skyrmion technology to the ultimate atomically thin limit. In this work, we theoretically demonstrate the Dzyaloshinskii–Moriya interaction and the formation of a Néel-type skyrmion lattice at the $CrTe_2/WTe_2$ bilayer van der Waals heterostructure. Our calculations suggest a field-controlled Néel-type skyrmion lattice – ferromagnet transition cycle. In addition, a spin-torque induced by spin-polarized current injection was simulated in order to study the motion of a skyrmion on a racetrack, where an increase of the skyrmion Hall angle is observed at high temperatures. Consequently, this study suggests that generation and annihilation of skyrmions can be achieved with temperature or field control and also manipulate the velocity and the direction of

the Néel-type skyrmions, through ultra-low current densities and temperature, thus, shedding light to the general picture of magnetic skyrmion control and design on two-dimensional van der Waals heterostructures.

Magnetic skyrmions are swirling spin textures in magnetic materials [Fig. 1(a)].[1] In most systems, the creation and stabilization of skyrmions is determined by the Dzyaloshinskii-Moriya interaction (DMI).[2] There are five different types of magnetic skyrmions arise in these systems which correspond to their symmetries.[3-5] Magnetic field-driven evolution of isolated magnetic skyrmions and their lattices has been investigated theoretically.[3-5] These findings describe that at high fields, the magnetic skyrmion lattices correspond to the global minimum of the system and their formation is typically observed through a first-order magnetic field-induced phase transition from the helical phase. In addition, skyrmion lattice transforms into an ensemble of isolated skyrmions which exist in the saturated state via a second-order phase transition, and offer two cases of evolution with decreasing the applied magnetic field. Either they condense into skyrmion lattices below a critical applied field, or they remain as localized states in the metastable saturated phase and convert into helical states. Magnetic skyrmions might offer a unique opportunity to bring topology into electronic devices for information storage and communications technology. The most promising applications are: (i) Skyrmion racetrack memory,[6-8] where the solitonic character of skyrmions is exploited and the information can be coded by a sequence of individual skyrmions in a magnetic track. (ii) Skyrmionic logic devices,[9,10] which rely on the fact that a skyrmion can be regarded as an independent particle, has given rise to the proposal of several skyrmion-based logic devices. (iii) Skyrmion radio-frequency devices,[11-14] where it has been proposed that the skyrmion breathing mode induced by spin-torques can be used to generate a radio-frequency signal.

Magnetic skyrmions were initially identified in single crystals magnetic compounds with a no inversion symmetry[15,16] and justified the existence of DMI induced by spin–orbit coupling (SOC). Skyrmions were then observed in inversion-symmetric ultrathin magnetic films epitaxially grown on heavy metals (HMs), formed due to large DMIs induced by the breaking of inversion symmetry at the interface and to the strong SOC of the neighboring HM.[17-19]

Since the occurrence of skyrmions depends on the strength of the DMI, a practical way to generate DMI is to construct heterostructures with spin ordering and strong SOC. Inversion symmetry is always broken at the interface of two dissimilar materials in a heterostructure, which is essential for generating DMI.[20-22] Two-dimensional (2D) van der Waals (vdW) magnets are a new and largely unexplored class of magnets that hold many advantages compared to common magnetic materials, since the study of magnetic skyrmions is pushed towards the 2D limit and due to their ease of creating heterostructures.[22-30] Néel-type skyrmions have been observed in mechanically exfoliated heterostructures of Fe_3GeTe_2 with WTe_2 topological material.[20] In addition, Cr_xTe_y 2D vdW ferromagnetic related compounds have intensively been studied by creating heterostructures with topological insulators.[31-33] Topological Hall effect, have been observed in Cr_2Te_3/Bi-bilayer, Cr_2Te_3/Bi_2Te_3 and $CrTe_2/Bi_2Te_3$ vdW heterostructures,[31-33] which is considered as evidence for magnetic skyrmions at the interfaces, yet there is no direct observation of them up to date. These findings were assisted by atomic-scale spin simulations, which however lack support from first-principles calculations.

In this work, by using first-principles calculations and atomic-scale spin simulations, we show that, that primarily $CrTe_2/WTe_2$ and to a lesser extend $CrTe_2/MoTe_2$ bilayer vdW heterostructure, create an interfacial DMI strong enough to stabilize magnetic skyrmion lattice. Our simulations also suggest a magnetic field-controlled Néel-type skyrmion lattice – ferromagnet transition cycle.

In addition, our results indicate that the skyrmion lattice is robust against thermal fluctuations at temperatures close to the Curie temperature. Moreover, a spin-torque induced by ultra-low spin-polarized current densities was simulated in order to study the motion of a skyrmion on a racetrack, where larger skyrmion Hall angle is observed at 80 K compared to 0 K, an effect which can be experimentally observed at liquid nitrogen temperatures. Therefore, our study shows that we can generate and annihilate skyrmions in a controlled way via temperature or magnetic field and control the velocity and the direction of the Néel-type skyrmions, through ultra-low spin-current densities and temperature.

Side and top views of the $CrTe_2/WTe_2$ 2D van der Waals heterostructure is shown in Figs. 1(b)-(d), obtained from first-principles calculations. $CrTe_2$ ferromagnet belongs to the 2D layered 1T octahedral family of transition metal dichalcogenides (TMDs) with space group $P\bar{3}m1$ (No. 164) where one Cr sublayer is sandwiched between two Te sublayers. The magnetic moment m is 3.0 μ_B/Cr.[31-33] On the other hand, bulk WTe_2 adopts an orthorhombic $Pmn2_1$ T_d structure. In the limit of a single layer has been predicted and experimentally verified to be 2D topological insulator (or quantum spin Hall insulator) and possesses one of the largest SOC amongst other TMDs,[34,35] while the bulk WTe_2 material becomes a topological type-II Weyl semimetal as first predicted[36] and later verified.[37] The lattice mismatch value (<1%) between $CrTe_2$ and WTe_2 is actually rather small compared to other heterostructures which report values around 3-4%,[29,30] thus we can safely neglect the influence of interfacial strain. Therefore, we placed WTe_2 directly on-top of $CrTe_2$ in a supercell with lattice constants a = 3.797 Å and b = 6.576 Å as indicated in Fig. 1(b).

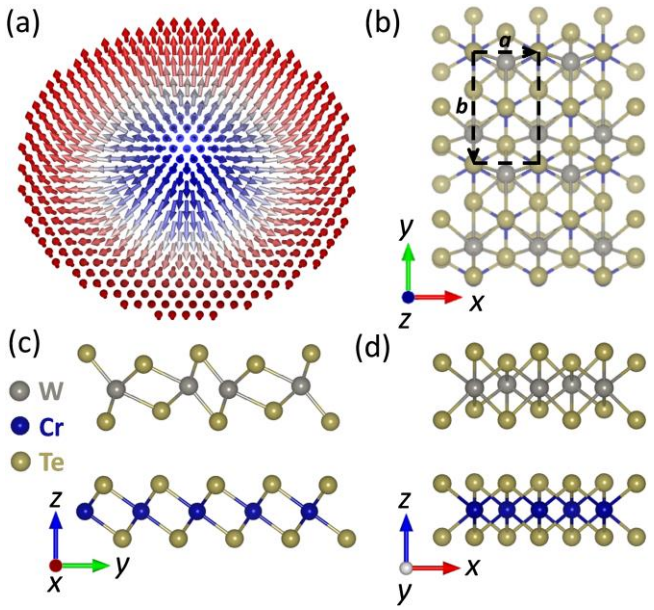

FIG. 1. (a) Schematic illustration of a skyrmion. (b)-(d) Side and top views of $CrTe_2/WTe_2$ vdW heterostructure.

Fe_3GeTe_2/WTe_2 heterostructures have shown skyrmion formation due to large DMI.[22] In addition, WTe_2 has theoretically predicted and experimentally demonstrated to possess large charge to spin conversion efficiency with spin Hall angle $\theta_{SH} = 0.17 – 1.0$,[38-41] making it a promising candidate for current-driven skyrmion manipulation with low-energy consumption.[1] On the other hand, few studies on the metastable topological T_d phase of the related compound $MoTe_2$,[42] report values of spin Hall angle smaller compared to WTe_2,[38,43] making it less studied and tested for spintronic applications.[22,30,39-41]

In a free standing $CrTe_2$ the DMI is absent due to the presence of inversion symmetry, however, at the interface of an heterostructure the inversion symmetry is broken (see Fig. S1 of supplementary material) and an interfacial DMI arises, making the formation of skyrmions possible. More details regarding the stacking of the heterostructure and broken inversion symmetry at the $CrTe_2/WTe_2$ heterostructure can be found in supplementary material.

In order to verify whether the skyrmion formation is possible in the $CrTe_2/WTe_2$ heterostructure, atomistic spin simulations have been performed using the *Spirit* package.[44] To account for the magnetic interactions of Cr atoms, the following atomically resolved Hamiltonian is considered:

$$H = -\sum_i m_i B \cdot n_i - \sum_i \sum_j K_i \left(\widehat{K}_j \cdot n_i\right)^2 - \sum_{\langle ij \rangle} J_{ij} n_i \cdot n_j - \sum_{\langle ij \rangle} D_{ij} \cdot \left(n_i \times n_j\right) \tag{1}$$

here at each lattice site *i* the spin direction is denoted by n_i, such that the magnetic moment is $m_i = \mu_i n_i$, *B* is the applied magnetic field, *K* the perpendicular anisotropy constant, *J* the exchange coupling constant and *D* the DMI. The spin dynamics are described by the LLG equation:[45,46]

$$\begin{aligned} \frac{\partial n_i}{\partial t} = &-\frac{\gamma}{(1+a^2)\mu_i} n_i \times B_i^{eff} - \frac{\gamma a}{(1+a^2)\mu_i} n_i \times \left(n_i \times B_i^{eff}\right) \\ &- \frac{\gamma a}{(1+a^2)\mu_B} u n_i \times (\hat{j}_e \cdot \nabla_r) n_i + \frac{\gamma}{(1+a^2)\mu_B} u n_i \times [n_i \times (\hat{j}_e \cdot \nabla_r) n_i] \end{aligned} \tag{2}$$

where γ is the electron gyrometric ratio, α = 0.05 is the damping parameter, the effective field $B_i^{eff} = -\partial H / \partial n_i$ and *u* is spin-torque defined as:

$$u = j_e P \hbar \mu_B / (2 e M_s) \tag{3}$$

with j_e the spin-polarized current density, *P* is the current polarization, ħ is Planck's reduced constant, *e* the electron charge and M_s the magnetization saturation. The effective field containing a stochastic thermal field $B_i^{eff} \rightarrow B_i^{eff} + B_i^{th}$ is given by:

$$B_i^{th}(t) = \sqrt{2D_i}\eta_i(t) = \sqrt{2ak_B T \frac{\mu_i}{\gamma}}\eta_i(t) \tag{4}$$

where η_i is white noise.[44]

The Hamiltonian parameters *K*, *J* and *D* are obtained from density functional theory (DFT) calculations. The first-principles calculations were performed using the Vienna Ab Initio Simulation Package (VASP).[47,48] The generalized-gradient approximation with Perdew-Burke-

Ernzerhof parametrization was used as the exchange correlation functional.[49] The kinetic energy cutoff was set at 500 eV, employing a Gamma-centered 18 × 10 × 1 *k*-point mesh. A Hubbard parameter U_{eff} = 3 eV has been applied on Cr *d* orbitals, using the Dudarev approach[50] in order to obtain a magnetic moment of 3.0 μ_B/Cr.[31-33] The atomic positions and lattice parameters were fully optimized by conjugate gradient, until the energy and force converge to 10^{-8} eV and 10^{-3} eV $Å^{-1}$, respectively. The vdW corrections were included by applying DFT-D3 Grimme's method[51] and a vacuum of 20 Å was used, in order to avoid interaction between the periodically repeated slabs. Spin-orbit coupling was used in all calculations.

The magnetic anisotropy *K* is defined as $K = E_{100} - E_{001}$, where E_{100} and E_{001} are the total energies with magnetization directions parallel and perpendicular to the plane of $CrTe_2$ film, respectively. The magnetic exchange *J* is proportional to the energy difference between antiferromagnetic (AFM) and ferromagnetic (FM) spin configurations i.e., $J = (E_{AFM} - E_{FM})/12$.[28,30,52] The DMI strength *D* is determined by mapping the total energies of artificially imposed spin configurations to the Hamiltonian $H = \sum_{\langle ij \rangle} D_{ij} \cdot (n_i \times n_j)$.[28,30,53,54] The in-plane component D_{12}^x between the spin site 1 and spin site 2 (n_1 and n_2), perpendicular to Cr-Cr bonds, can be calculated by setting the following four spin configurations: (i) $n_1 = (0,n,0)$, $n_2 = (0,0,n)$, (ii) $n_1 = (0,n,0)$, $n_2 = (0,0,-n)$, (iii) $n_1 = (0,-n,0)$, $n_2 = (0,0,n)$, (iv) $n_1 = (0,-n,0)$, $n_2 = (0,0,-n)$. The energies of the four spin configurations are denoted as E_1, E_2, E_3, and E_4, where the D_{12}^x can be calculated by $D_{12}^x = (E_1 + E_4 - E_2 - E_3)/4$. Therefore, the values of the Hamiltonian parameters obtained from first-principles calculations are summarized as *K* = 19 μeV, *J* = 11.53 meV and *D* = 0.64 meV. The positive values of *K, J* and *D* indicate out-of-plane magnetic anisotropy, ferromagnetic coupling and anticlockwise magnetization rotation from site 1 to site 2, respectively. The DMI value that is

obtained from the first-principles calculations is comparable to the values reported in the literature for other 2D vdW materials which range from 0.2 up to 2 meV.[23-30]

External stimuli play critical role to the spin texture and properties of a magnet. Few interesting transitions, including skyrmion-(bi)meron or skyrmion-antiskyrmion controlled by temperature or applied magnetic field, have extensively been studied.[28,30,55,56] A systematic investigation of the effect of applied magnetic field and temperature on the spin texture of Cr atoms of $CrTe_2/WTe_2$ 2D vdW heterostructure is performed, where we propose a field-controlled skyrmion lattice – ferromagnet transition cycle [Fig. 2].

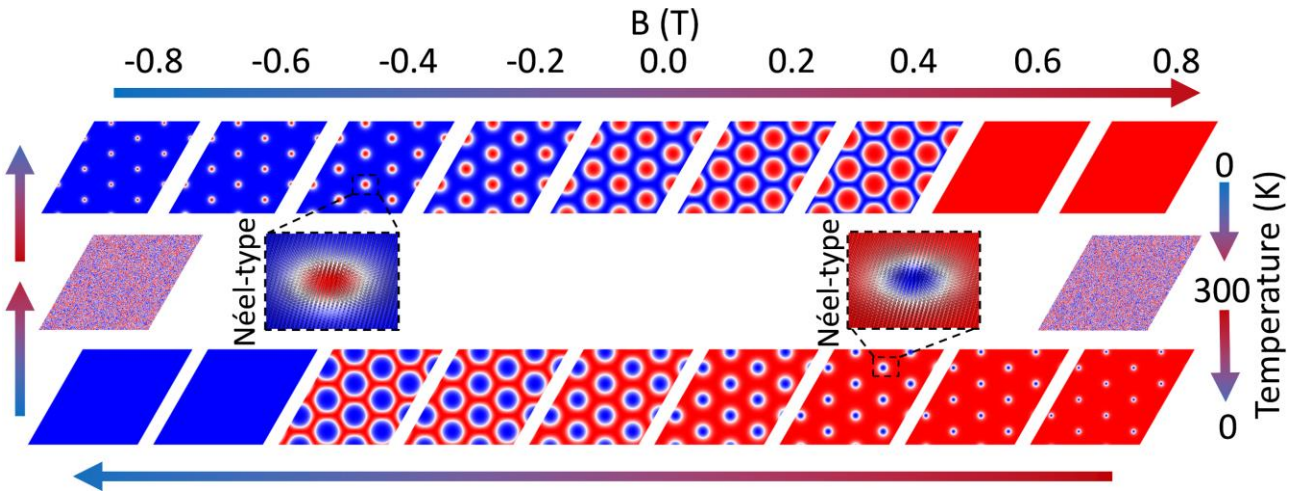

FIG. 2. A complete transition cycle of spin texture from -0.8 T to 0.8 T.

A complete cycle with an external applied field along *z* axis from -0.8 to 0.8 T on a 300×300 supercell is imaged in Fig. 2. Under a perpendicular applied field of -0.8 T, a Néel-type skyrmion lattice state becomes the ground state of the system. While the applied magnetic field approaches to positive values, the skyrmion diameter increases, until the field reaches 0.6 T, were the nearest neighboring skyrmions merge and the configuration converts to a ferromagnetic state. By setting and keeping the field at 0.8 T, we raised the temperature up to 300 K and then cool it down in order to excite skyrmions from the ferromagnetic state, where again a reversed, with respect to the

initial, Néel-type skyrmion lattice is formed which further turns to a ferromagnetic state at -0.6 T. Heating succeeded by rapid cooling is a process, that has extensively been used experimentally, but also theoretically, in order to obtain skyrmions.[30,57-59]

Isolated skyrmions can exist at zero applied magnetic field[1,3] if the DMI becomes smaller than a critical value $D_c = 2\sqrt{2JK}/\pi$,[3,60,61] while for DMI higher than D_c, isolated skyrmions should arise at applied magnetic fields higher than the transition field between skyrmion lattice and ferromagnetic phase.[4] However, in our case, where the interfacial DMI (0.64 meV) of the $CrTe_2/WTe_2$ vdW bilayer is larger than the critical value D_c = 0.42 meV, no isolated skyrmions were observed within the saturated phase as expected.

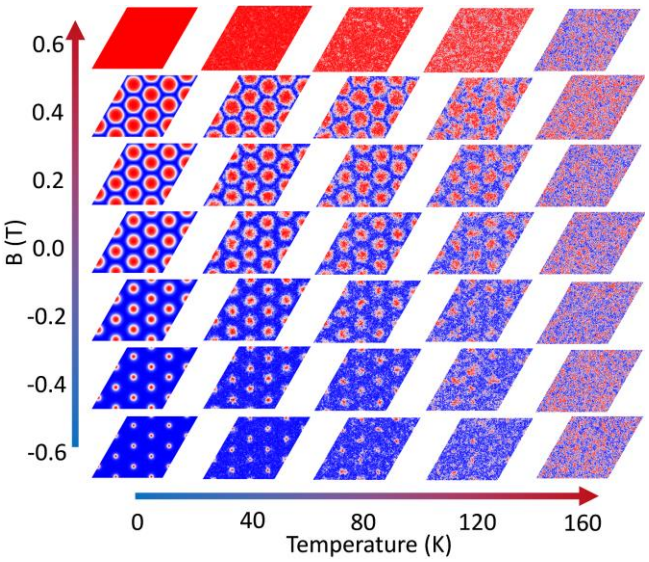

FIG. 3. Skyrmion phase diagram as a function of temperature and magnetic field.

In Fig. 3 is summarized a phase diagram of spin texture as a function of out-of-plane applied magnetic field B and temperature. The well-rounded skyrmions at 0 K become significantly deformed as the temperature is increased, due to thermal noise. While the applied magnetic field approaches to positive values, skyrmions show robustness against the thermal fluctuations due to the increase of the skyrmion diameter. The skyrmion lattice configuration dissolves and $CrTe_2$

becomes paramagnetic for the whole magnetic field range when it approaches the Curie temperature T_c = 163 K. Therefore, from Figs. 2 and 3 it is concluded that both applied field and temperature can act as a write and delete mechanisms of skyrmions on the $CrTe_2/WTe_2$ 2D vdW heterostructure.

Although the work has focused on the better performing $CrTe_2/WTe_2$ bilayer, the above DFT calculations and atomic scale spin simulations were also performed for the $CrTe_2/MoTe_2$ 2D vdW heterostructure. A smaller DMI value of 0.48 meV was obtained, leading to a Néel-type skyrmion lattice, which is less robust to both applied magnetic field and temperature. The results are summarized in Figs. S2 and S3 of supplementary material.

Magnetic skyrmions can be moved by low current densities.[30,62-68] The flexible deformation of skyrmions' shape due to the topological protection allows skyrmions during the current-driven motions to avoid impurities. We placed a Néel-type skyrmion under an out-of-plane applied magnetic field of 0.2 T on a $CrTe_2/WTe_2$ racetrack to study the spin-polarized current-induced motion of skyrmions. The spin-torque induced by spin current injection was simulated by using the Eq. (3). The skyrmion motion driven by the spin-torque can be described by a modified Thiele equation:[1,30,62,65]

$$G \times v - a\boldsymbol{\mathcal{D}} \cdot v + 4\pi\boldsymbol{\mathcal{B}} \cdot j_e = 0 \quad (5)$$

Here G = (0, 0, $-4\pi Q$) is the gyromagnetic coupling vector, with the topological charge $Q = 1/4\pi \int m \cdot (\partial_x n \times \partial_y n) d_x d_y$, $v = (v_x, v_y)$ is the skyrmion drift velocity along the x and y axes, respectively, $\boldsymbol{\mathcal{D}}$ is the dissipative force tensor, which depends on the domain wall width of the skyrmion, and $\boldsymbol{\mathcal{B}}$ is the tensor related to the spin-torque driving force. The first term is a Magnus force equivalent to the Lorentz force for charge carriers, giving rise to a Hall-like behavior of skyrmions, namely the skyrmion Hall effect. The second term is the dissipative force that is

associated to the intrinsic magnetic damping of a moving skyrmion, and the third term is the driving force from the spin-torque.

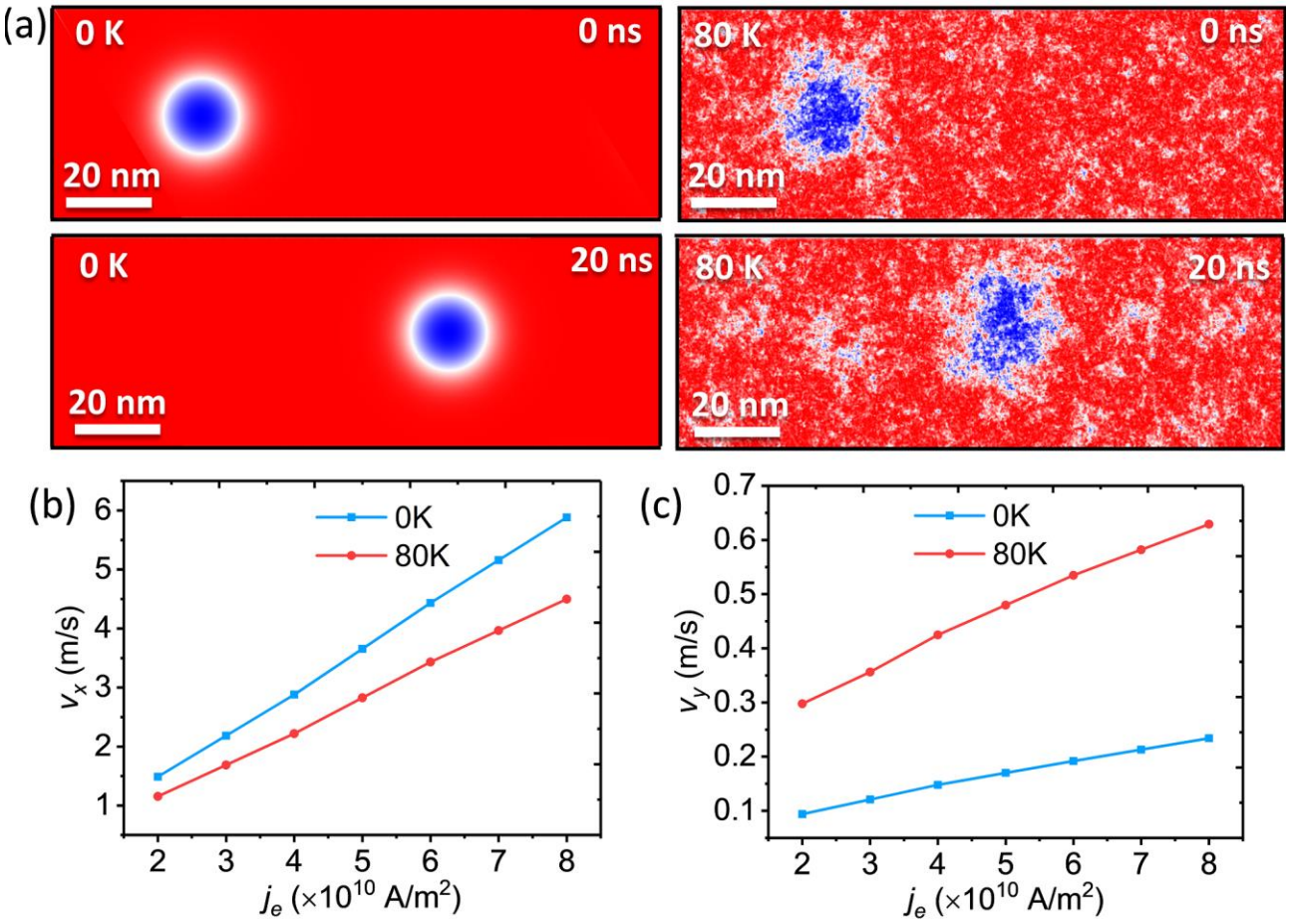

FIG. 4. (a) Screenshots of Néel-type skyrmion motion at 0 and 80 K, under the same spin-polarized current density $j_e = 4\times10^{10}$ A/m^2. (b) and (c) v_x and v_y as a function of j_e, respectively.

Figure 4(a) shows screenshots of the current-driven motion of a Néel-type skyrmion at 0 and 80 K, under the same spin current density $j_e = 4\times10^{10}$ A/m^2 polarized along x direction. The velocities are v_x = 2.88 m/s, v_y = 0.15 m/s at 0 K and v_x = 2.22 m/s, v_y = 0.42 m/s at 80 K. The skyrmion velocity as a function of spin current density j_e is illustrated at Figs. 4 (b) and (c). The v_x is reduced at 80 K, however, the v_y component of the Néel-type skyrmion velocity is increased, an effect which can be observed at liquid nitrogen temperature. This in agreement with a previous study,

stating that the skyrmion Hall angle increases with temperature, due to the side jump motion that the skyrmions experience by the Magnus force that pushes them away from equilibrium, while they continuously moving over thermal fluctuations, producing a finite value of skyrmion hall angle, with a magnitude that increases with larger driving forces and temperatures.[68] We also found that the critical current density to move a skyrmion is $\sim 0.9 \times 10^{10}$ A/m^2. The applied spin-polarized current densities to generate skyrmion motion in the $CrTe_2/WTe_2$ 2D vdW heterostructure are up to two orders of magnitude smaller from those required to drive skyrmionic bubbles in synthetic multilayer films,[1] thus making it a promising system for current-driven skyrmion manipulation with low-energy consumption.

In summary, by using DFT calculations in the $CrTe_2/WTe_2$ bilayer vdW heterostructure we obtained the perpendicular anisotropy constant, the exchange coupling constant and the DMI and introduce them to atomic-scale spin simulations. We found that, the interfacial DMI of the heterostructure is strong enough to stabilize magnetic skyrmions. In addition, we engineered a field-controlled Néel-type skyrmion lattice – ferromagnet transition cycle, where the skyrmion lattice is robust against thermal fluctuations close to T_c. We placed a Néel-type skyrmion on a racetrack to study the spin-polarized current-induced motion of skyrmions. The skyrmion velocity as a function of spin-polarized current density j_e indicates larger skyrmion Hall angle at 80 K compared to 0 K, an effect which can be observed at liquid nitrogen temperature. Our study shows that generation and annihilation of skyrmions in the $CrTe_2/WTe_2$ bilayer vdW heterostructure, can be achieved by controlling the applied field or the temperature and that the velocity and the direction of the skyrmions can be manipulated by ultra-low spin-polarized currents and temperature control.

SUPPLEMENTARY MATERIAL

See Supplementary Material for more details on stacking of the $CrTe_2/WTe_2$ heterostructure and Cr-Te bonds, and on atomic scale spin simulations on $CrTe_2/MoTe_2$ heterostructure.

ACKNOWLEDGMENTS

This work was supported by the Horizon 2020 projects SKYTOP – "Skyrmion-Topological Insulator and Weyl Semimetal Technology" (Grant No. 824123) and MSCA ITN SMART-X (Grant No. 860553).

AUTHOR DECLARATIONS

Conflict of Interest

The authors declare that they have no competing interests.

DATA AVAILABILITY

The data that support the findings of this study are available from the corresponding authors upon reasonable request.

REFERENCES

[1] A. Fert, N. Reyren, and V. Cros, Nat. Rev. Mater. **2**, 17031 (2017).

[2] I. E. Dzyaloshinskii, Sov. Phys. JETP **19**, 960 (1964).

[3] A. Bogdanov and A. Hubert, J. Magn. Magn. Mater. **138**, 255 (1994).

[4] A. O. Leonov, T. L. Monchesky, N. Romming, A. Kubetzka, A. N. Bogdanov, and R. Wiesendanger. N. J. Phys. **18**, 065003 (2016).

[5] A. N. Bogdanov and C. Panagopoulos, Nat. Rev. Phys. **2**, 492–498 (2020).

[6] J. Sampaio, V. Cros, S. Rohart, A. Thiaville, and A. Fert, Nat. Nanotechnol. **8**, 839–844 (2013).

[7] R. Tomasello, E. Martinez, R. Zivieri, L. Torres, M. Carpentieri, and G. Finocchio, Sci. Rep. **4**, 6784 (2014).

[8] W. Kang, Y. Huang, C. Zheng, W. Lv, N. Lei, Y. Zhang, X. Zhang, Y. Zhou, and W. Zhao, Sci. Rep. **6**, 23164 (2016).

[9] Y. Zhou and M. Ezawa, Nat. Commun. **5**, 8 (2014).

[10] X. Zhang, M. Ezawa, and Y. Zhou, Sci. Rep. **5**, 9400 (2015).

[11] J.-V. Kim, F. Garcia-Sanchez, J. Sampaio, C. Moreau-Luchaire, V. Cros, and A. Fert, Phys. Rev. B **90**, 064410 (2014).

[12] M. Carpentieri, R. Tomasello, R. Zivieri, and G Finocchio, Sci. Rep. **5**, 16184 (2015).

[13] G. Finocchio, M. Ricci, R. Tomasello, A. Giordano, M. Lanuzza, V. Puliafito, P. Burrascano, B. Azzerboni, and M. Carpentieri, *Appl. Phys. Lett.* **107**, 262401 (2015).

[14] F. Garcia-Sanchez, N. Reyren, J. Sampaio, V. Cros, and J.-V. Kim, New J. Phys. **18**, 075011 (2016).

[15] A. Fert and P. M, Levy, Phys. Rev. Lett. **44**, 1538–1541 (1980).

[16] A. Fert, Mater. Sci. Forum 59–60, 439–480 (1990).

[17] S. Heinze, K. von Bergmann, M. Menzel, J. Brede, A. Kubetzka, R. Wiesendanger, G. Bihlmayer, and S. Blügel, Nat. Phys. **7**, 713 (2011).

[18] N. Romming, C. Hanneken, M. Menzel, J. E. Bickel, B. Wolter, K. von Bergmann, A. Kubetzka, and R. Wiesendanger, Science **341**, 636 (2013).

[19] H. Yang, A. Thiaville, S. Rohart, A. Fert, and M. Chshiev, Phys. Rev. Lett. **115**, 267210 (2015).

[20] A. N. Bogdanov and U. K. Rößler, Phys. Rev. Lett. **87**, 037203 (2001).

[21] M. Bode, M. Heide, K. von Bergmann, P. Ferriani, S. Heinze, G. Bihlmayer, A. Kubetzka, O. Pietzsch, S. Blügel, and R. Wiesendanger, Nature **447**, 190 (2007).

[22] Y. Wu, S. Zhang, J. Zhang, W. Wang, Y. L. Zhu, J. Hu, G. Yin, K. Wong, C. Fang, and C. Wan, Nat. Commun. **11**, 3860 (2020).

[23] Q. Cui, J. Liang, Z. Shao, P. Cui, and H. Yang, Phys. Rev. B **102**, 094425 (2020).

[24] C. Xu, P. Chen, H. Tan, Y. Yang, H. Xiang, and L. Bellaiche, Phys. Rev. Lett. **125**, 037203 (2020).

[25] M. J. Meijer, J. Lucassen, R. A. Duine, H. J. Swagten, B. Koopmans, R. Lavrijsen, and M. H. Guimarães, Nano Lett. **20**, 8563 (2020).

[26] M.-G. Han, J. A. Garlow, Y. Liu, H. Zhang, J. Li, D. DiMarzio, M. W. Knight, C. Petrovic, D. Jariwala, and Y. Zhu, Nano Lett. **19**, 7859 (2019).

[27] D. Amoroso, P. Barone, and S. Picozzi, Nat. Commun. **11**, 5784 (2020).

[28] W. Sun, W. Wang, H. Li, G. Zhang, D. Chen, J. Wang, and Z. Cheng, Nat. Commun. **11**, 5930 (2020).

[29] C.-K. Li, X.-P. Yao, and G. Chen, G. Phys. Rev. Res. 3, L012026 (2021).

[30] W. Sun, W. Wang, J. Zang, H. Li, G. Zhang, J. Wang, and Z. Cheng, Adv. Funct. Mater. **31**, 2104452 (2021).

[31] J. Chen, L. Wang, M. Zhang, L. Zhou, R. Zhang, L. Jin, X. Wang, H. Qin, Y. Qiu, J. Mei, F. Ye, B. Xi, H. He, B. Li, and G. Wang, Nano Lett. **19**, 6144 (2019).

[32] L. Zhou, J. Chen, X. Chen, B. Xi, Y. Qiu, J. Zhang, L. Wang, R. Zhang, B. Ye, P. Chen, X. Zhang, G. Guo, D. Yu, J.-W. Mei, F. Ye, G. Wang, and H. He, ACS Appl. Mater. Interfaces **12**, 25135 (2020).

[33] X. Zhang, S. C. Ambhire, Q. Lu, W. Niu, J. Cook, J. S. Jiang, D. Hong, L. Alahmed, L. He, R. Zhang, Y. Xu, S. S.-L. Zhang, P. Li, and G. Bian, ACS Nano **15**, 15710 (2021).

[34] X. Qian, J. Liu, L. Fu, and J. Li, Science **346**, 1344 (2014).

[35] S. Tang, C. Zhang, D. Wong, Z. Pedramrazi, H.-Z. Tsai, C. Jia, B. Moritz, M. Claassen, H. Ryu, S. Kahn, J. Jiang, H. Yan, M. Hashimoto, D. Lu, R. G. Moore, C.-C. Hwang, C. Hwang, Z. Hussain, Y. Chen, M. M. Ugeda, Z. Liu, X. Xie, T. P. Devereaux, M. F. Crommie, S.-K. Mo, and Z.-X. Shen, Nat. Phys. **13**, 683 (2017).

[36] A. Soluyanov, D. Gresch, Z. Wang, Q. S. Wu, M. Troyer, X. Dai, and B. A. Bernevig, Nature **527**, 495 (2015).

[37] Y. Wu, D. Mou, N. H. Jo, K. Sun, L. Huang, S. L. Bud'ko, C. Canfield, and A. Kaminski, Phys. Rev. B **94**, 121113 (2016).

[38] J. Zhou, J. Qiao, A. Bournel, and W. Zhao, Phys. Rev. B **99**, 060408(R) (2019).

[39] B. Zhao, D. Khokhriakov, Y. Zhang, H. Fu, B. Karpiak, A. M. Hoque, X. Xu, Y. Jiang, B. Yan, and S. P. Dash, Phys. Rev. Res. **2**, 013286 (2020).

[40] Y. Fan, H. Li, DC. Mahendra, T. Peterson, J. Held, P. Sahu, J. Chen, D. Zhang, A. Mkhoyan, and J.-P. Wang, APL Mater. **8**, 041102 (2020).

[41] I. Shin, W. J. Cho, E.-S. An, S. Park, H.-W. Jeong, S. Jang, W. J. Baek, S. Y. Park, D.-H. Yang, J. H. Seo, G.-Y. Kim, M. N. Ali, S.-Y. Choi, H.-W. Lee, J. S. Kim, S. D. Kim, and G.-H. Lee, *Adv. Mater*. 2101730 (2021).

[42] K.-A. N. Duerloo, Y. Li, and E. J. Reed, Nat. Commun. **5**, 4214 (2014).

[43] C. K. Safeer, N. Ontoso, J. Ingla-Aynés, F. Herling, V. T. Pham, A. Kurzmann, K. Ensslin, A. Chuvilin, I. Robredo, M. G. Vergniory, F. de Juan, L. E. Hueso, M. R. Calvo, and F. Casanova, Nano Lett. **19** (12), 8758-8766 (2019).

[44] G. P. Müller, M. Hoffmann, C. Dißelkamp, D. Schürhoff, S. Mavros, M. Sallermann, N. S. Kiselev, H. Jónsson, and S. Blügel, Phys. Rev. B **99**, 224414 (2019).

[45] L. Landau and E. Lifshitz, Phys. Z. Sowjet. **8**, 153 (1935).

[46] T. L. Gilbert, IEEE Trans. Magn. **40**, 3443 (2004).

[47] G. Kresse and J. Furthmüller, Comput. Mater. Sci. **6**, 15 (1996).

[48] G. Kresse and J. Furthmüller, Phys. Rev. B **54**, 11169 (1996).

[49] J. P. Perdew, K. Burke, and M. Ernzerhof, Phys. Rev. Lett. **77**, 3865 (1996).

[50] S. L. Dudarev, G. A. Botton, S. Y. Savrasov, C. J. Humphreys, and A. P. Sutton, Phys. Rev. B **57**, 1505 (1998).

[51] S. Grimme, J. Antony, S. Ehrlich, and H. Krieg, Chem. Phys. **132**, 154104 (2010).

[52] M. T. Hutchings and E. J. Samuelsen, Phys. Rev. B **6**, 3447 (1972).

[53] H. J. Xiang, E. J. Kan, S.-H. Wei, M.-H. Whangbo, and X. G. Gong, Phys. Rev. B **84**, 224429 (2011).

[54] C. Xu, J. Feng, S. Prokhorenko, Y. Nahas, H. Xiang, L. Bellaiche, Phys. Rev. B **101**, 060404(R) (2020).

[55] H. Jani, J.-C. Lin, J. Chen, J. Harrison, F. Maccherozzi, J. Schad, S. Prakash, C.-B. Eom, A. Ariando, and T. Venkatesan, Nature **590**, 74 (2021).

[56] L. Peng, R. Takagi, W. Koshibae, K. Shibata, K. Nakajima, T.-H. Arima, N. Nagaosa, S. Seki, X. Yu, and Y. Tokura, Nat. Nanotechnol. **15**, 181 (2020).

[57] H. Oike, A. Kikkawa, N. Kanazawa, Y. Taguchi, M. Kawasaki, Y. Tokura, and F. Kagawa, Nat. Phys. **12**, 62 (2016).

[58] C. Jin, Z.-A. Li, A. Kovács, J. Caron, F. Zheng, F. N. Rybakov, N. S. Kiselev, H. Du, S. Blügel, and M. Tian, Nat. Commun. **8**, 15569 (2017).

[59] A. Chacon, L. Heinen, M. Halder, A. Bauer, W. Simeth, S. Mühlbauer, H. Berger, M. Garst, A. Rosch, and C. Pfleiderer, Nat. Phys. **14**, 936 (2018).

[60] A. N. Bogdanov and D. A. Yablonsky, Sov. Phys. JETP **68**, 101 (1989).

[61] A. N. Bogdanov, U. K. Rössler, and C. Pfleiderer, Physica B: Condensed Matter **359–361**, 1162–1164 (2005).

[62] J. Iwasaki, M. Mochizuki, and N. Nagaosa, Nat. Commun. **4**, 1463 (2013).

[63] W. Koshibae and N. Nagaosa, Sci. Rep. **8**, 6328 (2018).

[64] J. Iwasaki, M. Mochizuki, and N. Nagaosa, Nat. Nanotechnol. **8**, 742 (2013).

[65] W. Jiang, X. Zhang, G. Yu, W. Zhang, X. Wang, M. B. Jungfleisch, J. E. Pearson, X. Cheng, O. Heinonen, K. L. Wang, Y. Zhou, A. Hoffmann, and S. G. E. te Velthuis, Nat. Phys. **13**, 162 (2017).

[66] D. Maccariello, W. Legrand, N. Reyren, K. Garcia, K. Bouzehouane, S. Collin, V. Cros, and A. Fert, Nat. Nanotechnol. **13**, 233 (2018).

[67] L. Peng, K. Karube, Y. Taguchi, N. Nagaosa, Y. Tokura, X. Yu, Nat. Commun. **12**, 6797 (2021).

[68] C. Reichhardt and C. J. O. Reichhardt, J. Phys.: Condens. Matter **31**, 07LT01 (2018).